Crystal growth, magnetic properties, and critical behavior of the itinerant ferromagnet $K_{0.79}Co_2S_2$

Xiaoming Chen [1,2] Lei Duan [1,*] Linqian Liu,[1] Jianfa Zhao [2,3] Guangyang Dai [4,†] Wenmin Li [4] Xiancheng Wang,[2,3,‡] and Changqing Jin[2,3,5]

[1]*School of Materials Science and Engineering, Henan University of Technology, Zhengzhou 450007, China*

[2]*Beijing National Laboratory for Condensed Matter Physics, Institute of Physics, Chinese Academy of Sciences, Beijing 100190, China*

[3]*School of Physics, University of Chinese Academy of Sciences, Beijing 100190, China*

[4]*Institute of Quantum Materials and Physics, Henan Academy of Sciences, Zhengzhou 450046, China*

[5]*Materials Research Laboratory at Songshan Lake, Dongguan 523808, China*

(Received 17 June 2025; revised 28 September 2025; accepted 3 November 2025; published 1 December 2025)

In this paper, we successfully grow layered single-crystal $K_{0.79}Co_2S_2$ and systematically investigate its crystal structure, magnetic properties, electrical transport, specific heat, and even magnetic critical behavior. Single-crystal x-ray diffraction measurements indicate that $K_{0.79}Co_2S_2$ crystallizes into a tetragonal structure with space group *I*4/*mmm* (No. 139) and lattice parameters of $a = b = 3.711(4)$ Å and $c = 13.140(2)$ Å. Physical properties measurements demonstrate that $K_{0.79}Co_2S_2$ displays a metallic behavior with a ferromagnetic phase transition at $T_C \approx 113$ K, which was confirmed by the anomaly in the vicinity of T_C that occurs in electrical transport and specific heat curves. The calculated Rhodes-Wolfarth ratio (≈1.56) reveals the itinerant ferromagnetic characteristic of $K_{0.79}Co_2S_2$. A set of critical exponents was generated to be $\beta = 0.3006(4)$ with $T_C \approx 113.3(6)$ K and $\gamma = 1.1802(4)$ with $T_C \approx 113.2(5)$ K based on the modified Arrott plot and $\delta = 5.18(7)$ is yielded using a critical isotherm analysis at T_C, revealing a three-dimensional critical behavior. The magnetic interaction is determined to be a three-dimensional long-range coupling with the magnetic exchange distance decaying as $J(r) \sim r^{-4.91}$. Furthermore, a maximum of the magnetic entropy change $-\Delta S_M^{\max}$ for the applied field parallel to the *ab* plane is estimated to be ≈2.51 J kg^{-1} K^{-1} around T_C.

DOI: 10.1103/qldn-9n1v

I. INTRODUCTION

Layered materials with the $ThCr_2Si_2$ structure (space group *I*4/*mmm*) exhibit very abundant and fascinating physical properties, such as superconductivity, heavy fermion behavior, and various magnetic ground states, and thus have attracted extensive attention in past decades [1–8]. The transition metal dichalcogenides AM_2X_2, where *A* denotes alkali metal or Tl element, *M* stands for Fe, Co, or Ni, and *X* represents S or Se, are one of the typical examples of the $ThCr_2Si_2$ structural compounds [9–11]. For example, the iron chalcogenides $A_xFe_{2-y}Se_2$, where numbers of vacancies usually happen in the *A* and Fe sites, transform from antiferromagnetic insulators into superconductors by tuning the iron content [12–13]. When substituting Fe by Ni completely, ANi_2Se_2 without Ni vacancy displays heavy fermion or superconducting behaviors, such as in KNi_2Se_2 and $TlNi_2Se_2$ [14–15].

For the Co-based chalcogenides ACo_2X_2, it is reported that all the magnetic moments of them are ferromagnetically arranged in the Co-*X* layers, but the various types of interlayer interaction result in a diversity of magnetic ground states [16–19]. For example, $TlCo_2Se_2$ exhibits an antiferromagnetic transition at $T_N \approx 150$ K with an incommensurate helical magnetic structure along the *c* axis, and the replacement of Se by S yields a collinear ferromagnetic state in the series of $TlCo_2Se_{2-x}S_x$ for $1.75 \leqslant x \leqslant 2$ [20–21]. When pressure is applied on single-crystal $TlCo_2S_2$, the ferromagnetic transition temperature T_C gradually increases and a structural phase transition occurs at 5.2 GPa [22]. Furthermore, $CsCo_2Se_2$ is reported to exhibit an A-type antiferromagnetic state, while KCo_2Se_2 and $RbCo_2Se_2$ undergo a ferromagnetic transition with $T_C \approx 74$ and 76 K [19], respectively. It seems that the intercalating *A* ions and interlayer distance of Co-*X* layers play a crucial part in the magnetic properties of the Co-based chalcogenides ACo_2X_2 [21,23].

However, for the series of ACo_2S_2 (A = K, Rb, Cs), only polycrystalline samples of them have been synthesized up to now and the comprehensive understanding of their magnetic properties still remains elusive [19,24]. Here, we report on the crystal growth, crystal structure, magnetic properties, electrical transport, specific heat, and even magnetic critical behavior of single-crystal $K_{0.79}Co_2S_2$, a member of the AM_2X_2 family with two-dimensional Co-S layers. $K_{0.79}Co_2S_2$ exhibits a ferromagnetic metallic behavior with an itinerant characteristic. The critical exponents (β, γ, and δ) derived through various methods are consistent, revealing a three-dimensional critical behavior, and the exchange distance follows a decay as $J(r) \sim r^{-4.92}$ with long-range spin interaction.

*Contact author: lei_duan@haut.edu.cn

†Contact author: daigy@hnas.ac.cn

‡Contact author: wangxiancheng@iphy.ac.cn

TABLE I. Crystallographic data for $K_{0.79}Co_2S_2$.

Formula, $K_{0.79}Co_2S_2$
Space group $I4/mmm$ (No. 139); temperature, 302(2) K
$a = b = 3.711(4)$ Å, $c = 13.140(2)$ Å; $\alpha = \beta = \gamma = 90^\circ$
$V = 1800.9(66)$ Å^3; $Z = 2$
Goodness of fit on F^2: 1.36(4)
Final R indexes (all data): $R_1 = 0.042(1)$, w$R_2 = 0.102(1)$

Site	Wyckoff	x	y	z	Occupancy	U(Å)
K	2*b*	0	0	1/2	0.79(4)	0.030(4)
Co	4*d*	1/2	0	3/4	1	0.014(9)
S	4*e*	1/2	1/2	0.6511(8)	1	0.014(5)

II. EXPERIMENTS

High-quality single-crystal $K_{0.79}Co_2S_2$ was grown by the self-flux method. High-purity lumps of K and powders of Co and S were used as the starting materials and mixed in a molar ratio of 1:5:5. Then, the mixture with a total mass of approximately 2 g was placed into an Al_2O_3 tube and then sealed in an evacuated quartz tube, heated to 673 K at the rate of 1 K/min and held for 5 h, and then warmed to 973 K at the rate of 2 K/min and held for 10 h. After that, it was heated up to 1423 K and maintained for 20 h. Before shutting down the furnace, the mixtures were slowly cooled to 973 K at a rate of 3 K/h to obtain good-quality single crystals. To protect the samples from reacting with air or water, all the synthesis processes were carried out in a high-purity Ar atmosphere. The single crystal is relatively air sensitive and its metallic luster would gradually darken when exposed to air for a few minutes.

The x-ray diffraction of single-crystal $K_{0.79}Co_2S_2$ was measured at room temperature by Mo $K\alpha$ radiation ($\lambda = 0.71073$ Å) generated on a Bruker D8 VENTURE diffractometer. The powder x-ray diffraction of single crystals was measured by Cu $K\alpha$ radiation ($\lambda = 1.541$ Å) generated on a Rigaku Ultima VI (3 kW) diffractometer at 40 kV and 20 mA. Energy-dispersive x-ray spectroscopy (EDX) measurements were performed to confirm the chemical composition of the single crystals. Magnetic properties were measured using a superconducting quantum interferometer (MPMS 3, Quantum Design Inc.) in the $H \| ab$ and $H \perp ab$ planes, respectively. The isothermal magnetization curves from 0 to 50 kOe were measured from 103 to 123 K. The electronic resistivity and specific heat measurements were performed on a physical property measurement system (PPMS-16T, Quantum Design Inc.).

III. RESULTS AND DISCUSSIONS

A. Crystal structure and physical properties

The crystal structure of our obtained single crystal was confirmed by the single-crystal x-ray diffraction measurements. Detailed refinement results and crystallographic data are listed in Table I. The results indicate that the chemical formula of the single crystal is $K_{0.79}Co_2S_2$, suggesting that the K sites exhibited deficiencies of 21%, and $K_{0.79}Co_2S_2$ exhibits a tetragonal structure with space group $I4/mmm$ and lattice parameters of $a = b = 3.711(4)$ Å and $c = 13.140(2)$ Å, which is consistent with the reported polycrystalline sample [23]. Figure 1(a) exhibits the crystal structure of $K_{0.79}Co_2S_2$. It consists of the Co-S layers along the *ab* plane, which is formed by edge-sharing CoS_4 tetrahedra and separated by nonmagnetic K ions, thus exhibiting a strong quasi-two-dimensional structure. The x-ray diffraction (XRD) spectrum for the single-crystal $K_{0.79}Co_2S_2$ is displayed in Fig. 1(b) and the diffraction peaks are indexed. Only the diffraction peaks (0 0 *l*) are found and then suggest that the crystal surface is parallel to the *ab* plane. A picture of platelike single crystals with a size of $2 \times 2 \times 0.2$ mm^3 is shown in the inset of Fig. 1(b). Furthermore, the chemical composition of the single crystal was characterized using EDX at several different areas on the surface, as presented in Fig. 1(c). The average atomic ratio of K:Co:S is estimated to be 0.82:2.00:2.01, which is close to that obtained by single-crystal x-ray diffraction. An accompanying scanning electron microscopy (SEM) image of a $K_{0.79}Co_2S_2$ single crystal is provided in the inset of Fig. 1(c), exhibiting an obvious layered structure.

The magnetic susceptibility $\chi(T)$ as a function of temperature for single-crystal $K_{0.79}Co_2S_2$ was measured with the magnetic field (H) parallel or perpendicular to the *ab* plane, which is exhibited in Figs. 2(a) and 2(b), respectively. For the $H \| ab$ plane, $\chi(T)$ measured in both the field-cooling and zero-field-cooling models is overlapped in the entire measured range of temperature. With decreasing temperature,

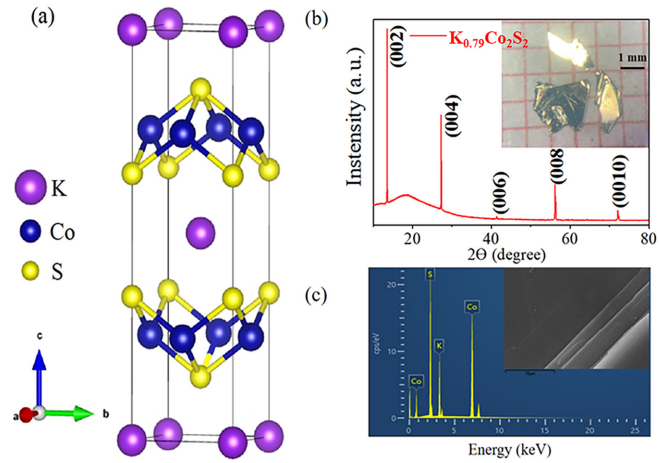

FIG. 1. (a) Crystal structure of $K_{0.79}Co_2S_2$. (b) XRD of the single-crystal $K_{0.79}Co_2S_2$; the inset shows a picture of $K_{0.79}Co_2S_2$. (c) Energy-dispersive x-ray spectrum collected on the single-crystal $K_{0.79}Co_2S_2$.

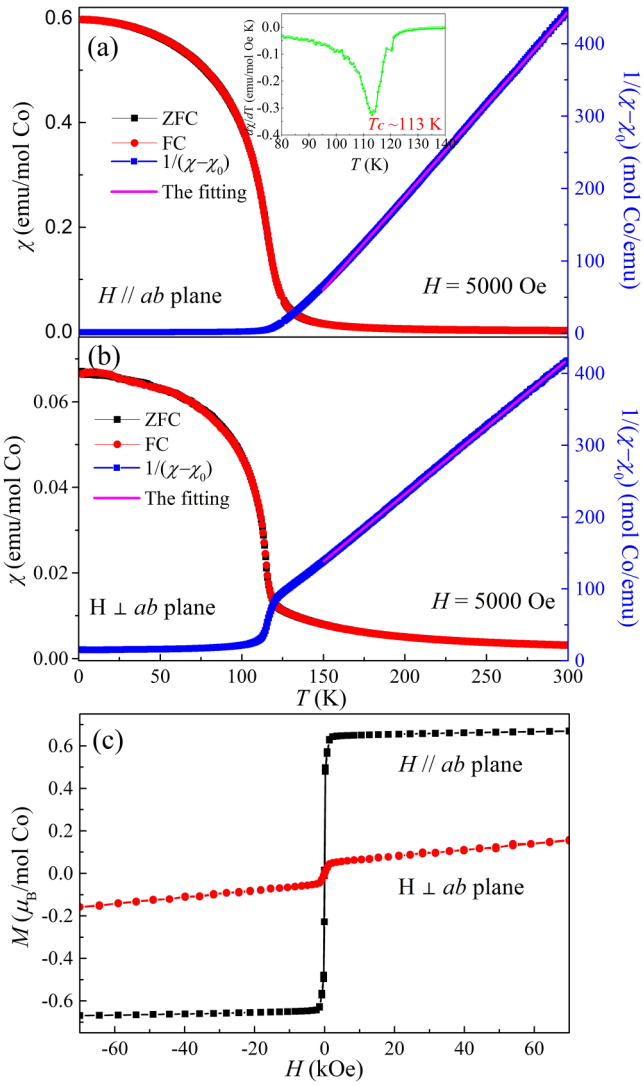

FIG. 2. Temperature dependence of the magnetization $\chi(T)$ of single-crystal KCo_2S_2 measured for the (a) $H \parallel ab$ plane and (b) $H \perp ab$ plane. The inverse susceptibility $1/(\chi-\chi_0)$ is shown in the right-hand axis. (c) Isothermal magnetization at 5 K.

$\chi(T)$ quickly increases at $T_C \approx 113$ K, which is determined by the temperature derivative of $\chi(T)$, displayed in the inset of Fig. 2(a), and tends to be saturated at low temperatures with the value of about 0.60 emu/mol Co, indicating a ferromagnetic transition. The $\chi(T)$ at high temperatures can be fitted well by the modified Curie-Weiss law $\chi = \chi_0 + C/(T-\Theta)$, where χ_0 is the susceptibility independent of temperature, Θ denotes the Weiss temperature, and C presents the Curie constant. By fitting $\chi(T)$ from 150 to 300 K, the values of χ_0, Weiss temperature Θ_{ab}, and Curie constant C can be estimated to be 1.01×10^{-4} emu/mol Co, 126.01 K, and 0.3918 emu K/mol Co, respectively. The inverse of magnetic susceptibility, $1/(\chi-\chi_0)$, is also presented in Fig. 2(a). According to the formula $\mu_{\text{eff}} = \sqrt{8C}\mu_B$, the effective moment μ_{eff} per Co atom can be calculated to be $1.77\mu_B$/Co. As shown in Fig. 2(b), the $\chi(T)$ for the $H \perp ab$ plane displays similar behavior to those for the $H \parallel ab$ plane, with a quick increase at 113 K and the saturated value of 0.067 emu mol^{-1}, which is almost ten times smaller than that for the $H \parallel ab$ plane. A fit for $\chi(T)$ by modified Curie-Weiss law from 150 to 300 K gives rise to $\chi_0 \approx 7.32 \times 10^{-4}$ emu mol^{-1} Co^{-1}, Weiss temperature $\Theta_c \approx 76.52$ K, and Curie constant $C \approx 0.5322$ emu K mol^{-1} Co^{-1}, respectively. Figure 2(b) also exhibits the inverse of magnetic susceptibility, $1/(\chi-\chi_0)$, for the $H \perp ab$ plane. The effective moment μ_{eff} is estimated to be $\approx 2.06\mu_B$/Co. The positive values of Θ_{ab} and Θ_c indicate that the dominant interactions both between the adjacent Co-S layers and within the same layer are ferromagnetic. The value of Θ_c is obviously derived from the T_C and $\Theta_{ab}/\Theta_c \approx 2$, suggesting the strength of intralayer interaction between Co atoms is stronger than that of interlayer interaction. Furthermore, the effective moments μ_{eff} for both $H \parallel ab$ and $H \perp ab$ planes are smaller than the theoretical value ($\approx 3.87\mu_B$) of a free Co^{2+} ion with $S = 3/2$, indicating the itinerant character of the Co ion in $K_{0.79}Co_2S_2$. Figure 2(c) displays the isothermal magnetization measured at 5 K with H parallel and perpendicular to the ab plane, respectively. The magnetization for $H \parallel ab$ exhibits a sharp increase above 1000 Oe and then tends to be saturated with the saturated moment $\mu_S \approx 0.66\mu_B$/Co, suggesting the ferromagnetic nature, while for $H \perp ab$, it does not saturate even at $H = 7$ T, which suggests a high anisotropy of $K_{0.79}Co_2S_2$ and that the ab plane is more easily magnetized. Moreover, with the obtained μ_{eff} and μ_S, we can calculate the Rhodes-Wolfarth ratio (RWR), quantified as the ratio of μ_C and μ_S, where μ_C is associated with the number of moving carriers and calculated from the formula $\mu_{\text{eff}}^2 = \mu_C(\mu_C + 2)$. For a localized system with ferromagnetic behavior, the RWR should be equal to 1, whereas RWR > 1 indicates the existence of itinerant ferromagnetism. Here, the value of RWR is calculated to be 1.56 for $H \parallel ab$, indicating the itinerant ferromagnetism in $K_{0.79}Co_2S_2$.

Figure 3(a) presents the temperature dependence of the electrical resistivity of single-crystal $K_{0.79}Co_2S_2$, measured with the applied current (I) parallel to the ab plane. The electrical resistivity displays a metallic behavior with the resistivity about 0.36 mΩ cm at room temperature. As the temperature decreases, a rapid decrease of the resistivity occurs at 113 K, which is determined by the temperature derivative of electrical resistivity, which is shown in left inset of Fig. 3(a). The anomaly in the resistivity curve agrees with the magnetic susceptibility curve, confirming the ferromagnetic transition. Furthermore, the resistivity ρ versus T^2 (K^2) from 2 to 80 K is presented in the right-hand inset of Fig. 3(a) and exhibits a linear behavior, indicating that the resistivity can be fitted using the equation $\rho = \rho_0 + AT^2$ [25], where ρ_0 denotes the residual resistivity, resulting from the lattice defects of the material, and the second term comes from the electron-phonon scattering. After fitting the resistivity in the low-temperature region, the parameters ρ_0 and A can be obtained to be 0.0397(3) mΩ cm and 8.44×10^{-6} mΩ cm K^{-2}, respectively. These results indicate that $K_{0.79}Co_2S_2$ follows Fermi liquid behavior in the low-temperature region.

Figure 3(b) presents the specific heat $Cp(T)$ curve for $K_{0.79}Co_2S_2$ measured from 2 to 200 K. An obviously small peak occurs at $T_C \approx 113$ K, suggesting a magnetic phase transition at this temperature. To extract the magnetic contribution C_m related to the phase transition, we first fitted the

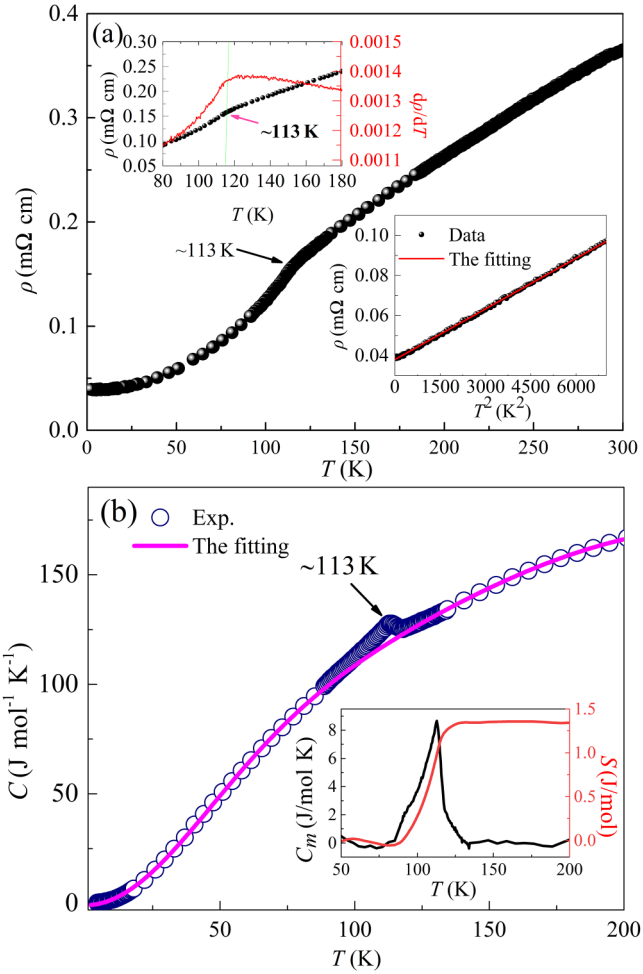

FIG. 3. (a) Temperature dependence of electrical resistivity for KCo_2S_2. The left-hand inset shows $d\rho/dT$ versus temperature; the right-hand inset shows ρ versus T^2 at low temperatures (2–80 K). (b) Specific heat versus temperature for KCo_2S_2 from 2 to 200 K. The blue curve represents the fitting using the Thirring model. The inset exhibits the magnetic contribution to the specific heat and the magnetic entropy.

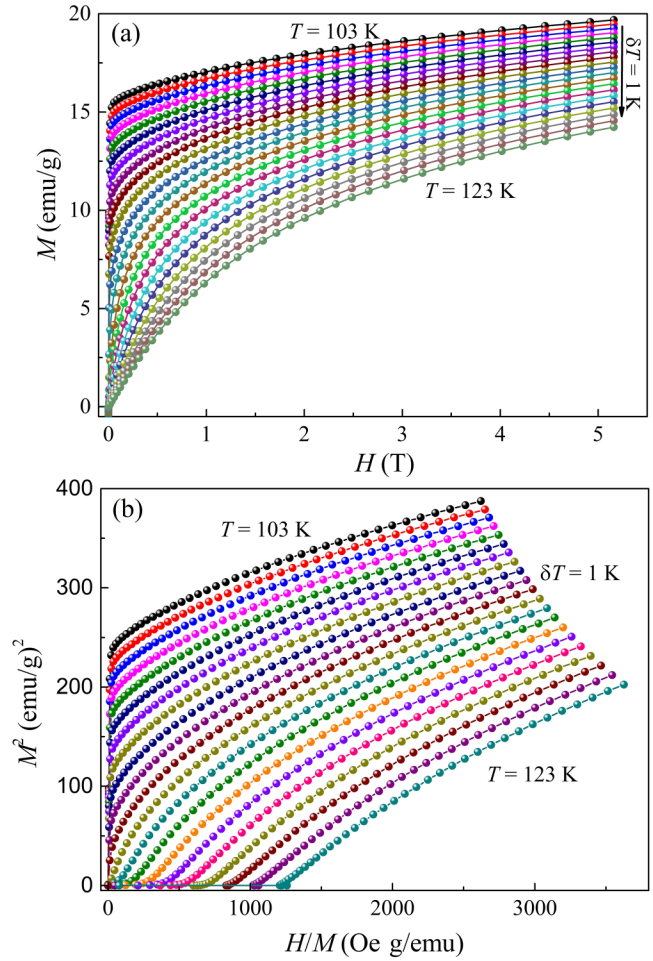

FIG. 4. (a) Isothermal magnetization curves of KCo_2S_2 measured from 103 to 123 K. (b) Arrott plots M^2 vs H/M.

$Cp(T)$ curve using the Thirring model to obtain the lattice contribution [26]. According to this model, the lattice contribution is expressed as $C_{\text{lat}} = 3NR(+\Sigma_{n=1}^{\infty} b_n \mu^{-n})$, where N denotes the number of atoms in the crystal cell, R is the ideal gas constant, and $\mu = (2\pi T/\theta_D)^2 + 1$, with θ_D being the Debye temperature. Sack *et al.* show that for a Debye solid with $T = \theta_D/4$, the model achieves an accuracy of ≈0.03% using only four terms [27,28]. Hence, we used $n = 4$ and gained a reasonable fitting as shown in Fig. 3(b). After subtracting the lattice contribution, the C_m is obtained and displayed in the inset of Fig. 3(b). A sharp peak occurs in the C_m curve at $T_C \approx 113$ K. The inset of Fig. 3(b) also exhibits the magnetic entropy estimated by integrating C_m/T, and the total magnetic entropy change ΔS resulting from the long-range magnetic ordering is obtained to be ≈1.35 J mol^{-1} K^{-1}, which is small and only 23.43% of $R\ln(2S+1) = 5.76$ J mol^{-1} K^{-1} with the spin $S = 1/2$ and R being the gas constant. The results indicate that the strong short-range order above T_C of $K_{0.79}Co_2S_2$ is formed and then results in the release of most of the magnetic entropy, which is a common phenomenon in two-dimensional layered systems such as $CrGeTe_3$ [29] and $Mn_3Si_2Te_6$ [30].

B. Critical behavior

For a ferromagnetic material with a second-order phase transition, investigating its magnetic critical behavior is considered a powerful method to understand the nature of its magnetism. Different magnetic critical behaviors usually are expressed by sets of various interrelated critical exponents (β, γ, and δ) [31,32], for example, $\beta = 0.364$ and $\gamma = 1.386$ for the three-dimensional (3D) Heisenberg model. Isothermal magnetization curves for $K_{0.79}Co_2S_2$ near T_C were measured in the range 103–123 K with a temperature interval $\Delta T = 1$ K along the *ab* plane and the results are exhibited in Fig. 4(a). Based on the isothermal magnetization data, we plotted the Arrott plots M^2 vs H/M, as shown in Fig. 4(b). All the slopes of Arrott plots are found to be positive, which suggests the nature of a second-order ferromagnetic phase transition near T_C of $K_{0.79}Co_2S_2$, according to the criterion proposed by Banerjee [33]. Furthermore, according to the mean-field theory, the M^2 vs H/M curves should be a series of parallel straight lines in the high-field region. However, as shown in

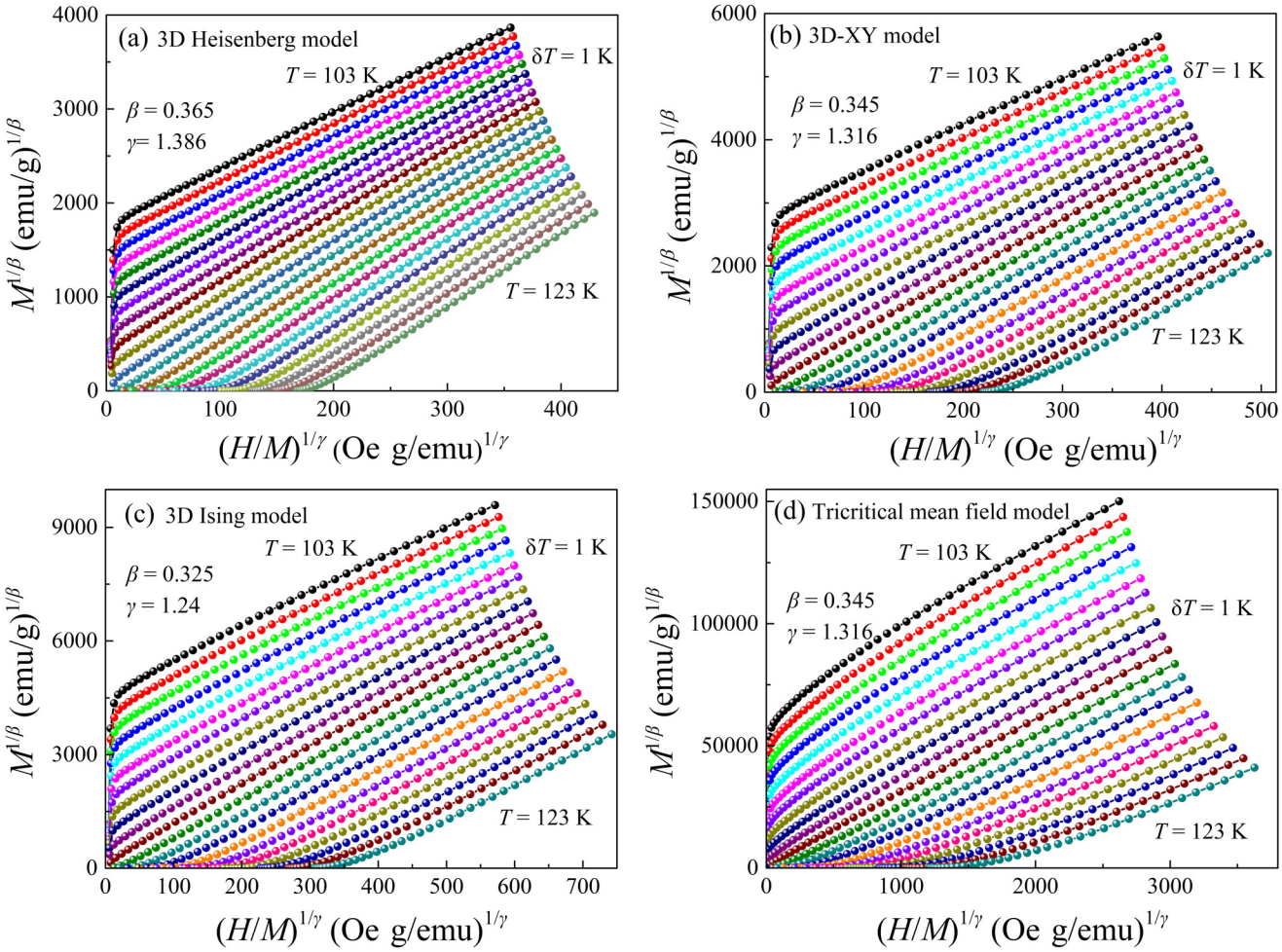

FIG. 5. The modified Arrott plots for different models: (a) 3D Heisenberg model, (b) 3D XY model, (c) 3D Ising model, and (d) tricritical mean-field model.

Fig. 4(b), in the Arrott plots, all the curves are observed to be nonlinear, which rules out the possibility of a mean-field model and so a modification of Arrott plots should be performed [32].

Figures 5(a)–5(d) display the modified Arrott plots $M^{1/\beta}$ vs $(H/M)^{1/\gamma}$ of $K_{0.79}Co_2S_2$ with the critical exponents of the 3D Heisenberg model ($\beta = 0.365$, $\gamma = 1.386$), 3D XY model ($\beta = 0.345$, $\gamma = 1.316$), 3D Ising model ($\beta = 0.325$, $\gamma = 1.24$), and tricritical mean-field model ($\beta = 0.25$, $\gamma = 1.0$). In the high-field region, the curves of the four models present quasistraight lines. In order to obtain the most appropriate model to describe the magnetic critical behavior of $K_{0.79}Co_2S_2$, the temperature dependence of normalized slopes (NS), defined as $\mathrm{NS} = S(T)/S(T_C)$ [31,32], where $S(T)$ is the slope of the modified Arrott plots $M^{1/\beta}$ vs $(H/M)^{1/\gamma}$ and $S(T_C)$ the slope when $T = T_C \approx 113$ K, are plotted in Fig. 6 for the above modes. The values of NS should be equal to 1.0 when the critical exponents are accurate. However, deviation of the four models occurs and indicates that any universal class of model is not suitable to describe the critical behavior of $K_{0.79}Co_2S_2$.

To determine more accurate critical exponents (β, γ, and δ), a rigorous iterative method was employed; the process has been described in detail in Ref. [34]. According to the

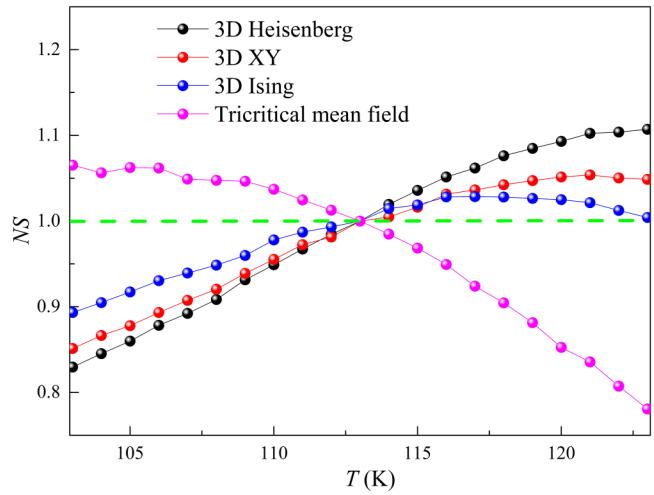

FIG. 6. The normalized slopes $\mathrm{NS} = S(T)/S(T_C)$ as a function of temperature for different modes.

scaling hypothesis, the critical exponents (β, γ, and δ) can be mathematically expressed as

$$M_s(T) = M_0(-\varepsilon)^{\beta} \quad (\varepsilon < 0,\ T < T_C), \tag{1}$$

$$\chi_0^{-1}(T) = (h_0/M_0)(-\varepsilon)^{\gamma} \quad (\varepsilon > 0,\ T > T_C), \tag{2}$$

$$M(H) = DH^{1/\delta} \quad (\varepsilon = 0,\ T = T_C), \tag{3}$$

where $\varepsilon = (T - T_C)/T_C$ represents the reduced temperature; M_0, h_0/M_0, and D denote the critical amplitudes; $M_s(T)$ is the spontaneous magnetization, determined by the intersection of the linear extrapolation line in high-magnetic-field parts of the $M^{1/\beta}$ vs $(H/M)^{1/\gamma}$ curves for $T < T_C$ and the $M^{1/\beta}$ axis; and the inverse of initial magnetic susceptibility, $\chi_0^{-1}(T)$, is the intersection of the linear extrapolation line of the $M^{1/\beta}$ vs $(H/M)^{1/\gamma}$ curves for $T > T_C$ and the $(H/M)^{1/\gamma}$ axis. After fitting $M_s(T)$ and $\chi_0^{-1}(T)$ by Eqs. (1) and (2), new critical exponents β and γ can be obtained and then used to construct new modified Arrott plots $M^{1/\beta}$ vs $(H/M)^{1/\gamma}$. The above procedures were iteratively performed until these critical exponents are converged. It should be noted that these final critical exponents acquired by this method are independent of the initial values of β and γ. Here, the 3D Ising model was used for the initial parameters, which then gave rise to the critical exponents $\beta = 0.3006(4)$ with $T_C^- \approx 113.3(6)$ K and $\gamma = 1.1802(4)$ with $T_C^+ \approx 113.2(5)$ K, after several of the above processes, which is displayed in Fig. 7(a).

Furthermore, the critical exponents and ferromagnetic transition temperature T_C can also be determined using the Kouvel-Fisher method [34]:

$$M_s(T)/[dM_s(T)/dT] = (T - T_C)/\beta, \tag{4}$$

$$\chi_0^{-1}(T)/[d\chi_0^{-1}(T)/dT] = (T - T_C)/\gamma. \tag{5}$$

Figure 7(b) exhibits the temperature dependence of $M_s/(dM_s/dT)$ and $\chi_0^{-1}/(d\chi_0^{-1}/dT)$, and the linear fitting gives rise to $\beta = 0.3022(3)$ with $T_C^- \approx 113.3(5)$ K and $\gamma = 1.1621(6)$ with $T_C^+ \approx 113.3(1)$ K, which is well consistent with those values obtained from the iterative method.

Figure 8 displays the isothermal magnetization at 113 K with the inset plotted on logarithmic scale. Based on Eq. (3), δ can be obtained. By the linear fit on the $\ln(M)$ vs $\ln(H)$ curve in the high-field region, which is exhibited in the inset of Fig. 8, the critical exponent δ is obtained to be 5.18(7). Furthermore, the critical exponent δ can also be estimated by the Widom scaling relation $\delta = 1 + \gamma/\beta$. Using the obtained values of β and γ through the Kouvel-Fisher method, δ is calculated to be 4.84(5), in agreement with the value obtained from Fig. 8.

In order to further evaluate the accuracy of the above analysis, we examine whether the critical exponents and T_C follow the scaling equation, which in the asymptotic critical region can be written as [35]

$$M(H, \varepsilon) = \varepsilon^{\beta} f_{\pm}\left(\frac{H}{\varepsilon^{\beta+\gamma}}\right), \tag{6}$$

where f represents the scaling function with f_+ for $T > T_c$ and f_- for $T < T_C$. Based on the above equation, if T_C and

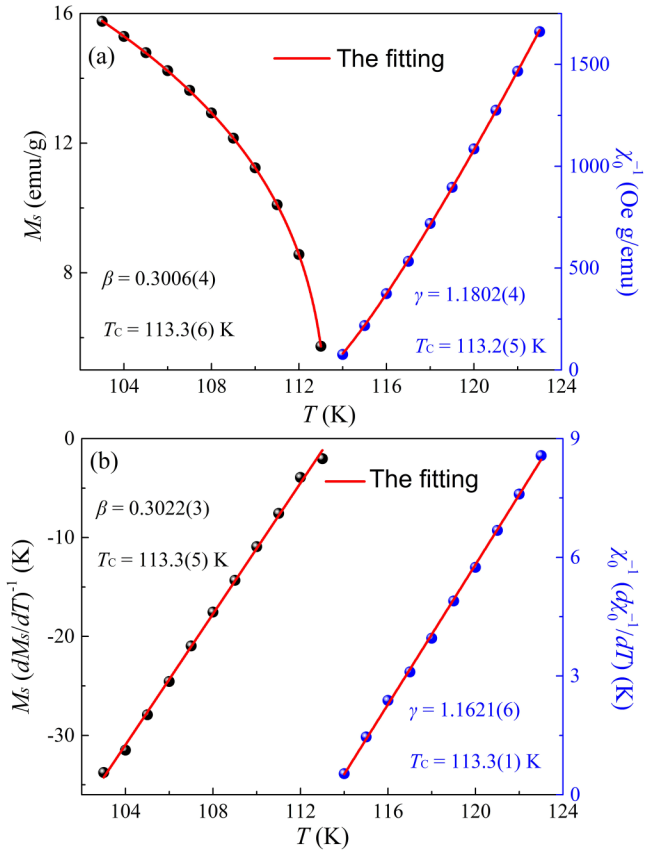

FIG. 7. Temperature dependence of the spontaneous magnetization $M_s(T)$ (left) and inverse initial susceptibility $\chi_0^{-1}(T)$ (right) of KCo_2S_2. The fitting results are displayed by the red curves. (b) Kouvel-Fisher plot for $M_s(T)(dM_s(T)/dT)^{-1}$ (left) and $\chi_0^{-1}(T)(d\chi_0^{-1}(T)/dT)^{-1}$ (right) with solid fit lines.

the critical exponents are reasonable, the curves of the renormalized magnetization $m \equiv \varepsilon^{-\beta} M(H, \epsilon)$ vs the renormalized field $h \equiv \varepsilon^{-(\beta+\gamma)} H$ should yield two generalized curves, one for $T > T_C$ and the other for $T < T_C$ [32,34]. Here, the critical exponents and T_C obtained by the Kouvel-Fisher method were used to plot m vs h. The results are shown in Fig. 9(a) and we can see that all the isothermal magnetization data converge into two universal curves. The corresponding ln-ln plot is displayed in the inset of Fig. 9(a), where all the curves also split into two separate branches below T_C and above T_C. Moreover, the m^2 vs h/m plot is a more rigorous method to further verify the critical exponents and T_C, which is plotted in Fig. 9(b). All the curves also collapse into two divided branches. Thus, the above scaling analyses further clarify that the critical exponents and T_C obtained from different methods are reliable.

Furthermore, it is crucial to study the nature of the magnetic interaction range in $K_{0.79}Co_2S_2$. The universal classes of the magnetic transition are dependent on the exchange interaction $J(r)$. According to the renormalization group theory, the long-range exchange interaction decays with distance r as $J(r) \sim r^{-(d+\sigma)}$, where d presents the dimensionality and σ is a positive constant associated with the range of the interaction.

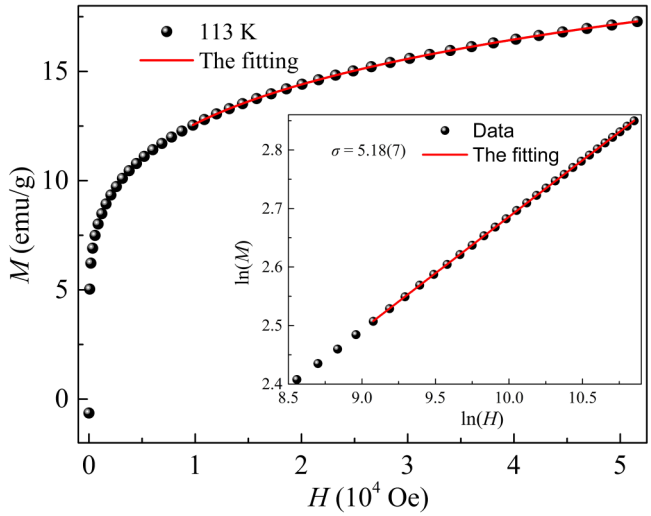

FIG. 8. Isothermal magnetization curve at 113 K with a red fitting curve. The inset shows the plot on ln-ln scale with a solid red fitting line.

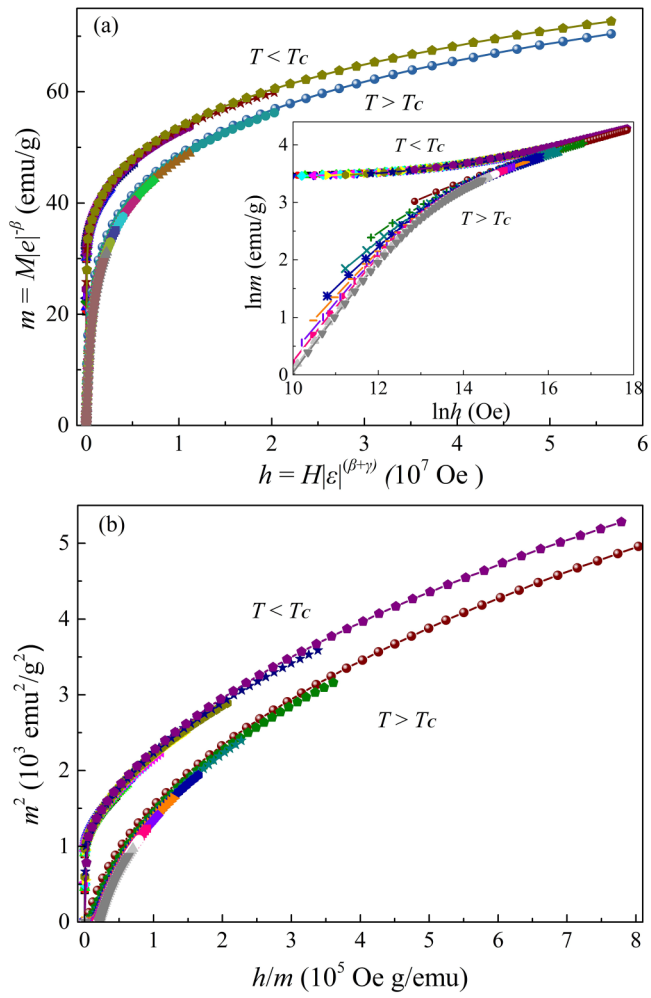

FIG. 9. (a) Scaling plots of renormalized magnetization m vs renormalized field h around T_C for KCo_2S_2. The inset displays the plot in ln-ln scale. (b) The m^2 vs h/m plot.

The value of σ can be determined from the formula

$$\gamma = 1 + \frac{4}{d}\left(\frac{n+2}{n+8}\right)\Delta\sigma + \frac{8(n+2)(n-4)}{d^2(n+8)^2}\left(1 + \frac{2G(\frac{d}{2})(7n+20)}{(n-4)(n+8)}\right)\Delta\sigma^2, \quad (7)$$

where n is the spin dimension, $\Delta\sigma = \sigma - d/2$, and $G(\frac{d}{2}) = 3 - \frac{1}{4}(\frac{d}{2})^2$. The system for $\sigma > 2$ can be described by the short-range Heisenberg model, where the magnetic interactions $J(r)$ decrease faster than r^{-5}, while for $\sigma \leqslant 3/2$, the long-range mean-field model is valid with $J(r)$ decaying slower than $r^{-4.5}$. To estimate the values of d, n, and σ in this system, which give rise to a value of γ close to that ($\gamma \approx 1.18$) obtained from the experiments, the procedure reported in Ref. [36] was performed. The other critical exponents can be estimated from the following scaling equations: $\nu = \gamma/\sigma$, $\alpha = 2 - \nu d$, $\beta = (2 - \alpha - \gamma)/2$, and $\delta = 1 + \gamma/\beta$, where ν and α denotes the critical exponents of correlation length. We repeated the process for a various series of $\{d, n\}$ and found that $\{d, n\} = \{3, 2\}$ and $\sigma = 1.92$ yield the critical exponents ($\beta = 0.369$, $\gamma = 1.315$, and $\delta = 4.56$), close to the experimental values determined from various methods. Thus, in the case of $K_{0.79}Co_2S_2$, the exchange interaction decays as $J(r) \sim r^{-4.92}$ with long-range spin interaction.

C. Magnetic entropy change

The magnetic entropy change $\Delta S_M(T, H)$ induced by the external field, which is an effective method to study phase transition, can be obtained by the following formula [31]:

$$\Delta S_M(T, H) = \int_0^H \left(\frac{\partial S}{\partial H}\right)_T dH = \int_0^H \left(\frac{\partial M}{\partial T}\right)_H dH, \quad (8)$$

where $(\frac{\partial S}{\partial H})_T = (\frac{\partial M}{\partial T})_H$ is derived from Maxwell's equations [31]. Owing to the magnetization strength measured at small discrete temperature and magnetic field intervals, $\Delta S_M(T, H)$ can be approximately determined as

$$\Delta S_M(T, H) = \frac{\int_0^H M(T_i, H)dH - \int_0^H M(T_{i+1}, H)dH}{T_i - T_{i+1}}. \quad (9)$$

Figure 10(a) exhibits the temperature dependence of the magnetic entropy change under various fields with the $H \parallel ab$ plane. All the curves display obviously broad peaks around T_C and the peaks shift toward higher temperature as the magnetic field increases, which rules out the mean-field model. Furthermore, the maximum of the magnetic entropy change, $-\Delta S_M^{\max}$, also increases with increasing magnetic field and reaches 2.51 $J\,kg^{-1}\,K^{-1}$ with the $H \parallel ab$ plane at 50 kOe, which is comparable with common two-dimensional ferromagnetic materials, such as 2.5 $J\,kg^{-1}\,K^{-1}$ in $Mn_3Si_2Te_6$ [37] and 3.28 $J\,kg^{-1}\,K^{-1}$ in $AlCMn_3$ [38]. For a second-order ferromagnetic material, the maximum of the magnetic entropy change, $-\Delta S_M^{\max}$, obeys a power-law dependence on the field as the following equation: $-\Delta S_M^{\max} \propto H^n$, where n at T_C is associated with the critical exponents and can be calculated by the equation $n(T_C) = 1 + (\beta - 1)/\beta + \gamma$. As shown

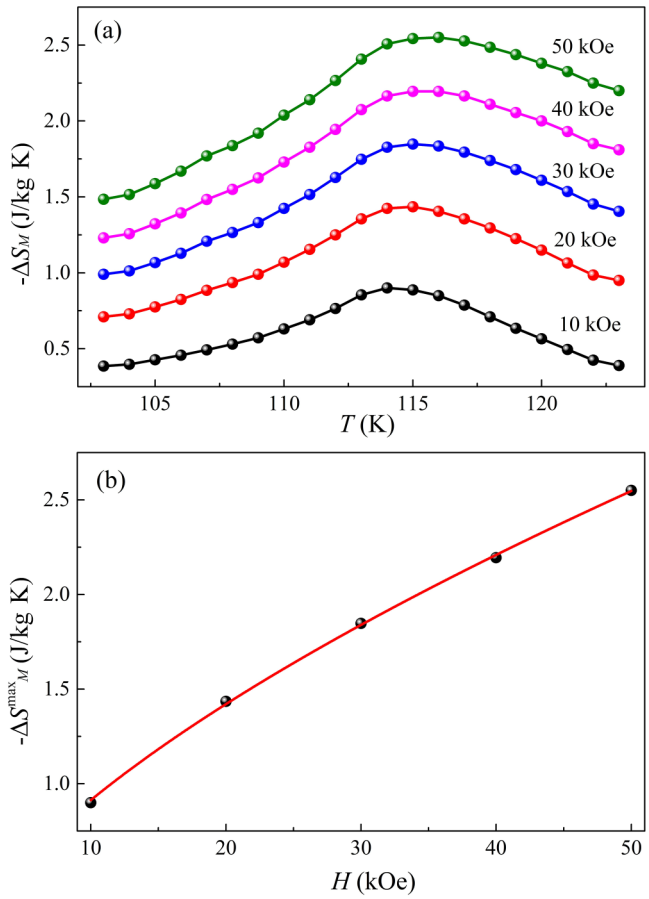

FIG. 10. (a) Temperature dependence of magnetic entropy change $-\Delta S_{\mathrm{M}}$ at various magnetic fields. (b) Field dependence of $-\Delta S_M^{\max}$ with the red fitting curve.

in Fig. 10(b), the value of n is calculated to be 0.461 by fitting the data, which is close to that (≈0.527) obtained by the modified Arrott plot.

D. Discussion

Layered ACo_2X_2 exhibits various magnetic ground states related to its interlayer coupling. $TlCo_2Se_2$ undergoes a helical magnetic structure, where the intralayer spins are ferromagnetically coupled while the interlayer spins spiral with an angle of ≈121° [20]. When $TlCo_2Se_2$ is doped with S at Se sites, it has been revealed that, in $TlCo_2Se_{2-x}S_x$, the interlayer spin spiral angle gradually decreases with increasing S doping level x, and a collinear ferromagnetic structure can be reached when $x > 1.75$ [21]. The magnetic critical behavior in $TlCo_2S_2$ has been studied, which indicates that $TlCo_2S_2$ displays a robust tricritical behavior [17]. When $TlCo_2S_2$ is slightly doped with Ni at Co sites, the ferromagnetic ground state of $Tl(Co_{0.95}Ni_{0.05})_2S_2$ changes to an antiferromagnetic one. In addition, a metamagnetic transition can be induced by magnetic field $H < 1.5$ T at 20 K, further indicating the possibility of the existence of a tricritical point in $Tl(Co_{0.95}Ni_{0.05})_2S_2$ [17]. Also, for $CsCo_2Se_2$, an antiferromagnetic-ferromagnetic-paramagnetic tricritical point has been observed in the T-H phase diagram [39]. In our case of $K_{0.79}Co_2S_2$, the critical exponents estimated from different methods and the theoretical values of some universal models are summarized in Table II. A comprehensive study by Taroni *et al.* suggests that for two-dimensional (2D) ferromagnetic materials, the critical exponent β should be located in a window $0.1 \leqslant \beta \leqslant 0.25$ [40]. The obtained value of β ($\approx 0.3006(4)$) reveals that $K_{0.79}Co_2S_2$ clearly displays a 3D critical behavior, indicating that the interlayer interaction cannot be neglected. By comparison, the obtained critical exponents $\beta \approx 0.3006(4)$ and $\gamma \approx 1.1802(4)$ are small and far from that expected for the 3D Heisenberg model or 3D XY model. Although these values are close to that for the 3D Ising model, it does not suggest that there would exist strong easy-axis anisotropy with moments directed out of the plane expected by the 3D Ising model due to the fact that easy-plane magnetization has been observed in $K_{0.79}Co_2S_2$. It is noted that the obtained critical exponents are closer to the values of the tricritical mean-field model relative to that for the 3D Heisenberg or 3D XY model. Considering that the tricritical point has been observed in both $TlCo_2S_2$ and $CsCo_2Se_2$, it is proposed that the tricritical point could emerge in the $K_{0.79}Co_2S_2$ system when changing the interlayer coupling by chemical doping. The critical behavior in $K_{0.79}Co_2S_2$ could be complicated and needs to be understood by combining both the 3D Heisenberg and 3D XY models and the tricritical mean-field model.

IV. CONCLUSION

Layered single-crystal $K_{0.79}Co_2S_2$ with $ThCr_2Si_2$-type structure has been successfully grown and its crystal structure,

TABLE II. Critical exponents of $K_{0.79}Co_2S_2$ derived from various methods (modified Arrott plot, Kouvel-Fisher method, and critical isotherm analysis) and some theoretical models.

	Technique	Ref.	T_C (K)	β	γ	δ
$K_{0.79}Co_2S_2$	Modified Arrott plot	This work	113.2(6)	0.3006(4)	1.1802(4)	$4.92(5)^{\mathrm{cal}}$
	Kouvel-Fisher method	This work	113.3(5)	0.3022(3)	1.1621(2)	$4.84(5)^{\mathrm{cal}}$
	Critical isotherm analysis	This work	113.0			5.18(7)
Mean-field model	Theory	[35]		0.5	1.0	3.0
3D Heisenberg model	Theory	[35]		0.365	1.386	4.8
3D Ising model	Theory	[35]		0.325	1.24	4.82
3D XY model	Theory	[35]		0.345	1.316	4.81
Tricritical mean-field model	Theory	[17]		0.25	1.0	5.0

transport, and magnetic properties have been systematically investigated. $K_{0.79}Co_2S_2$ demonstrates a metallic behavior with Fermi liquid behavior and undergoes a ferromagnetic transition at $T_C \approx 113$ K with an itinerant character. Analysis of the critical behavior through different methods generates a series of critical exponents $\beta = 0.3006(4)$ with $T_C^- \approx 113.3(6)$ K, $\gamma = 1.1802(4)$ with $T_C \approx 113.2(5)$ K, and $\delta = 5.18(7)$, and the scaling analysis confirms the reliability of these exponents. Renormalization group theory reveals a three-dimensional magnetic interaction of $K_{0.79}Co_2S_2$ decaying as $J(r) \sim r^{-4.92}$. The tricritical mean-field model is used to explain the deviation of the critical exponents from the expected values for the 3D Heisenberg or 3D XY model. Our results provide more ingredients to understand the magnetism and critical behavior in layered ACo_2X_2 materials. It is desired to look for the tricritical point in the $K_{0.79}Co_2S_2$ system by chemical doping in the future.

ACKNOWLEDGMENTS

We greatly appreciate the support of the National Natural Science Foundation of China under Grants No. 12404005, No. 12404008, No. 12204515, and No. 12474097, and the National Key R&D Program of China under Grants No. 2024YFA1408000 and No. 2023YFA1406000. This work was also supported by Beijing National Laboratory for Condensed Matter Physics (Grant No. 2023BNLCMPKF006) and the Cultivation Program for Young Backbone Teachers in Henan University of Technology (Grant No. 21421332).

DATA AVAILABILITY

The data that support the findings of this article are not publicly available. The data are available from the authors upon reasonable request.

[1] W. Y. Peng, S. Chanakian, and A. Zevalkink, Crystal chemistry and thermoelectric transport of layered AM_2X_2 compounds, Inorg. Chem. Front. **5**, 1744 (2018).

[2] X. X. Wang, W. Q. Wang, W. D. Hutchison, C. W. Wang, H. Y. Hao, F. Su, Y. F. Xue, J. C. Debnath, S. J. Campbell, Z. X. Cheng, and J. L. Wang, Magnetic structure, magneto-caloric properties and magnetic critical behaviours of $LaMn_2Ge_2$ compounds, J. Alloys Compd. **909**, 164784 (2022).

[3] X. Y. Wang, J. F. Lin, X. Y. Zeng, H. Wang, X. P. Ma, Y. Wang, K. Han, and T. L. Xia, Multiple magnetic phase transitions and critical behavior in single-crystal $SmMn_2Ge_2$, Chin. Phys. Lett. **40**, 067503 (2023).

[4] N. Kurita, M. Kimata, K. Kodama, A. Harada, M. Tomita, H. S. Suzuki, T. Matsumoto, K. Murata, S. Uji, and T. Terashima, High-pressure electrical resistivity measurements of $EuFe_2As_2$ single crystals, Phys. Rev. B **83**, 214513 (2011).

[5] F. Ronning, E. D. Bauer, T. Park, S.-H. Baek, H. Sakai, and J. D. Thompson, Superconductivity and the effects of pressure and structure in single-crystalline $SrNi_2P_2$, Phys. Rev. B **79**, 134507 (2009).

[6] Y. C. Wang, Y. J. Xu, Y. Liu, X. J. Han, X. G. Zhu, Y. F. Yang, Y. Bi, H. F. Liu, and H. F. Song, First-principles study of the role of surface in the heavy-fermion compound $CeRh_2Si_2$, Phys. Rev. B **103**, 165140 (2021).

[7] Y. Lai, J. Y. Chan, and R. E. Baumbach, Electronic landscape of the f-electron intermetallics with the $ThCr_2Si_2$ structure, Sci. Adv. **8**, eabp8264 (2022).

[8] X. B. Luo, Y. Zhang, Q. Y. Chen, Q. Liu, L. Z. Luo, S. Y. Tan, X. G. Zhu, and X. C. Lai, Electronic structure evolution accompanying heavy fermion formation in $CeCu_2Si_2$, Sci. China Phys. Mech. Astron. **63**, 287413 (2020).

[9] J. J. Ying, Z. J. Xiang, Z. Y. Li, Y. J. Yan, M. Zhang, A. F. Wang, X. G. Luo, and X. H. Chen, Physical properties of $A_xFe_{2-y}S_2$ (A = K, Rb, and Cs) single crystals, Phys. Rev. B **85**, 054506 (2012).

[10] X. C. Hong, Z. Zhang, S. Y. Zhou, J. Pan, Y. Xu, H. D. Wang, Q. H. Mao, M. H. Fang, J. K. Dong, and S. Y. Li, Multigap nodeless superconductivity in nickel chalcogenide $TlNi_2Se_2$, Phys. Rev. B **90**, 060504(R) (2014).

[11] U. D. Wdowik, G. Jagło, and D. Legut, Effect of cation-vacancy superstructure on the phonon dynamics in KNi_2Se_2, Phys. Rev. B **101**, 045125 (2020).

[12] S. S. Hou, A. Qian, X. Y. Zhang, S. Jiang, M. S. Tan, X. Y. Ma, W. Ren, S. Y. Wang, N. Zhang, J. W. Zhang, X. G. Qiu, A. M. Zhang, and Q. M. Zhang, Superconducting phase in $K_xFe_{2-y}Se_2$: Critical role of intact FeSe layers, Phys. Rev. B **112**, 014512 (2025).

[13] J. Hazi, T. Mousavi, P. Dudin, G. van der Laan, F. Maccherozzi, A. Krzton-Maziopa, E. Pomjakushina, K. Conder, and S. C. Speller, Magnetic imaging of antiferromagnetic and superconducting phases in $Rb_xFe_{2-y}Se_2$ crystals, Phys. Rev. B **97**, 054509 (2018).

[14] J. R. Neilson, A. Llobet, A. V. Stier, L. Wu, J. Wen, J. Tao, Y. Zhu, Z. B. Tesanovic, N. P. Armitage, and T. M. McQueen, Mixed-valence-driven heavy-fermion behavior and superconductivity in KNi_2Se_2, Phys. Rev. B **86**, 054512 (2012).

[15] H. D. Wang, C. H. Dong, Q. H. Mao, R. Khan, X. Zhou, C. X. Li, B. Chen, J. H. Yang, Q. P. Su, and M. H. Fang, Multiband superconductivity of heavy electrons in a $TlNi_2Se_2$ single crystal, Phys. Rev. Lett. **111**, 207001 (2013).

[16] H. Ryu, M. Abeykoon, K. F. Wang, H. C. Lei, N. Lazzrevic, J. B. Warren, E. S. Bozin, Z. V. Popovic, and C. Petrovic, Insulating and metallic spin glass in Ni-doped $K_xFe_{2-y}Se_2$ single crystals, Phys. Rev. B **91**, 184503 (2015).

[17] Q. H. Mao, J. H. Yang, H. D. Wang, B. Chen, X. D. Geng, M. Y. Pan, and M. H. Fang, From tricritical ferromagnetism to metamagnetism in quasi-two dimensional $Tl(Co_{1-x}Ni_x)_2S_2$ ($x = 0, 0.05$), J. Phys.: Condens. Matter **30**, 295801 (2018).

[18] J. Liu, J. Sheng, W. Luo, J. Wang, W. Bao, J. Yang, M. Fang, and S. A. Danilkin, A single-crystal neutron diffraction study on magnetic structure of $CsCo_2Se_2$, Chin. Phys. B **27**, 117401 (2018).

[19] J. Yang, B. Chen, H. Wang, Q. Mao, M. Imai, K. Yoshimura, and M. Fang, Magnetic properties in layered ACo_2Se_2 (A = K,

Rb, Cs) with the $ThCr_2Si_2$-type structure, Phys. Rev. B **88**, 064406 (2013).

[20] R. Lizárraga, S. Ronneteg, R. Berger, A. Bergman, P. Mohn, O. Eriksson, and L. Nordström, Theoretical and experimental study of the magnetic structure of $TlCo_2Se_2$, Phys. Rev. B **70**, 024407 (2004).

[21] S. Ronneteg, S. Felton, R. Berger, and P. Nordblad, Chemical tuning of the interlayer magnetic coupling in $TlCo_2Se_{2-x}S_x$, J. Magn. Magn. Mater. **299**, 53 (2006).

[22] L. Duan, X. Yao, Y. Peng, Y. Jia, Y. Wei, X. Chen, Y. Feng, S. Cai, S. Wang, Y. Liu, Z. Zhao, C. Jin, X. Liang, and J. Zhu, Pressure-induced anomaly of transport properties and structural transition in layered ferromagnetic metal $TlCo_2S_2$, J. Alloys Compd. **1009**, 176986 (2024).

[23] Z. N. Guo, H. H. Zhang, D. Wang, B. L. Han, S. F. Jin, and W. X. Yuan, Ferromagnetic interlayer interaction in $KCo_2Se_{2-x}S_x$ ($0 \leqslant x \leqslant 2$) and its chemical origin, Dalton Trans. **45**, 8248 (2016).

[24] G. Huan and M. Greenblatt, Antiferromagnetic-to-ferromagnetic transition in metallic $Tl_{1-x}K_xCo_2Se_2$ ($0 \leqslant x \leqslant 1.0$) with $ThCr_2Si_2$-type structure, J. Less Common Met. **156**, 247 (1989).

[25] J. Wang, J. Wu, T. Wang, Z. Xu, J. Wu, W. Hu, Z. Ren, S. Liu, K. Behnia, and X. Lin, *T*-square resistivity without Umklapp scattering in dilute metallic Bi_2O_2Se, Nat. Commun. **11**, 3846 (2020).

[26] H. Thirring, Zur Theorie der Raumgitterschwingungen und der spezifischen Wärme fester Körper, Phys. Z. **14**, 867 (1913).

[27] R. A. Sack, A. A. Maradudin, and G. H. Weiss, Extension of the range of validity of Thirring's expansion for the specific heat of crystals, Phys. Rev. **124**, 717 (1961).

[28] J. E. Gordon, M. L. Tan, R. A. Fisher, and N. E. Phillips, Specific heat data of high-T_c superconductors: Lattice and electronic contributions, Solid State Commun. **69**, 625 (1989).

[29] G. T. Lin, H. L. Zhuang, X. Luo, B. J. Liu, F. C. Chen, J. Yan, Y. Sun, J. Zhou, W. J. Lu, P. Tong, Z. G. Sheng, Z. Qu, W. H. Song, X. B. Zhu, and Y. P. Sun, Tricritical behavior of the two-dimensional intrinsically ferromagnetic semiconductor $CrGeTe_3$, Phys. Rev. B **95**, 245212 (2017).

[30] Y. Liu, Z. X. Hu, M. Abeykoon, E. Stavitski, K. Attenkofer, E. D. Bauer, and C. Petrovic, Polaronic transport and thermoelectricity in $Mn_3Si_2Te_6$ single crystals, Phys. Rev. B **103**, 245122 (2021).

[31] L. Duan, X. C. Wang, C. L. Guan, S. Wang, L. P. Shi, J. L. Zhu, J. Zhang, J. F. Zhao, Z. W. Zhao, C. J. Xiao, and C. Q. Jin, Critical behavior of the ferromagnetic metal La_3CrAs_5 with quasi-one-dimensional spin chains, J. Alloys Compd. **905**, 164214 (2022).

[32] L. Duan, X. C. Wang, J. Zhang, Z. Hu, J. F. Zhao, Y. G. Feng, H. L. Zhang, H.-J. Lin, C. T. Chen, W. Wu, Z. Li, R. Wang, J. F. Zhang, T. Xiang, and C. Q. Jin, Synthesis, structure, and magnetism in the ferromagnet La_3MnAs_5: Well-separated spin chains coupled via itinerant electrons, Phys. Rev. B **106**, 184405 (2022).

[33] S. K. Banerjee, On a generalised approach to first and second order magnetic transitions, Phys. Lett. **12**, 16 (1964).

[34] A. K. Pramanik and A. Banerjee, Critical behavior at paramagnetic to ferromagnetic phase transition in $Pr_{0.5}Sr_{0.5}MnO_3$: A bulk magnetization study, Phys. Rev. B **79**, 214426 (2009).

[35] S. N. Kaul, Static critical phenomena in ferromagnets with quenched disorder, J. Magn. Magn. Mater. **53**, 5 (1985).

[36] L. Z. Zhang, A.-L. Zhang, X.-D. He, X.-W. Ben, Q.-L. Xiao, W.-L. Lu, F. Chen, Z. Feng, S. Cao, J. Zhang, and J.-Y. Ge, Critical behavior and magnetocaloric effect of the quasi-two-dimensional room-temperature ferromagnet Cr_4Te_5, Phys. Rev. B **101**, 214413 (2020).

[37] Y. Liu and C. Petrovic, Critical behavior and magnetocaloric effect in $Mn_3Si_2Te_6$, Phys. Rev. B **98**, 064423 (2018).

[38] N. Ennassiri, N. Tahiri, O. El Bounagui, H. Ez-Zahraouy, and A. Benyoussef, Magnetic, magnetocaloric and transport properties in $AlCMn_3$ antiperovskite compound, J. Alloys Compd. **741**, 1196 (2018).

[39] F. von Rohr, A. Krzton-Maziopa, V. Pomjakushin, H. Grundmann, Z. Guguchia, W. Schnick, and A. Schilling, Field-induced transition of the magnetic ground state from A-type antiferromagnetic to ferromagnetic order in $CsCo_2Se_2$, J. Phys.: Condens. Matter **28**, 276001 (2016).

[40] A. Taroni, S. T. Bramwell, and P. C. W. Holdsworth, Universal window for two-dimensional critical exponents, J. Phys.: Condens. Matter **20**, 275233 (2008).